ORCA – Online Research @ Cardiff

1 # Global patterns and dynamics of climate-groundwater interactions

2

3 **Authors:** M.O. Cuthbert[1,2,3*], T. Gleeson[4], N. Moosdorf[5], K.M. Befus[6], A. Schneider[7],
4 J. Hartmann[8] and B. Lehner[9]

5 [1]School of Earth and Ocean Sciences, Cardiff University, Main Building, Cardiff, CF10 3AT,
6 UK

7 [2]Water Research Institute, Cardiff University, The Sir Martin Evans Building, Museum Ave,
8 Cardiff CF10 3AX, UK

9 [3]Connected Waters Initiative Research Centre, UNSW Sydney, NSW 2052, Australia

10 [4]Department of Civil Engineering and School of Earth and Ocean Sciences, University of
11 Victoria, PO Box 1700, ECS 316, 3800 Finnerty Road, Victoria, British Colombia, Canada
12 V8W 2Y2

13 [5]Leibniz Centre for Tropical Marine Research (ZMT), Fahrenheitstrasse 6, 28359 Bremen,
14 Germany

15 [6]Department of Civil and Architectural Engineering, University of Wyoming, Laramie,
16 Wyoming, USA 82071

17 [7]Sorbonne Université, CNRS, EPHE, Milieux environnementaux, transferts et interactions
18 dans les hydrosystèmes et les sols, METIS, F-75005 Paris, France

19 [8]Institute for Geology, Center for Earth System Research and Sustainability (CEN),
20 Universität Hamburg, Hamburg, Germany

21 [9]Department of Geography, McGill University, 805 Sherbrooke Street West, Montreal H3A
22 0B9, Quebec, Canada

23

24 *Correspondence and request for data sets can be sent to Mark Cuthbert at

25 cuthbertm2@cardiff.ac.uk

26

27

28   **Summary Paragraph**

29   Groundwater is the largest available store of global freshwater[1], upon which more than two

30   billion people rely[2]. It is therefore important to quantify the spatiotemporal interactions

31   between groundwater and climate. However, current understanding of the global scale

32   sensitivity of groundwater systems to climate change[3,4] – as well as the resulting variation in

33   feedbacks from groundwater to the climate system[5,6] - is limited. Here, using groundwater

34   model results in combination with hydrologic datasets, we examine the dynamic timescales

35   of groundwater system responses to climate change. We show that nearly half of global

36   groundwater fluxes could equilibrate with recharge variations due to climate change on

37   human (~100 year) timescales, and that areas where water tables are most sensitive to

38   changes in recharge are also those that have the longest groundwater response times. In

39   particular, groundwater fluxes in arid regions are shown to be less responsive to climate

40   variability than in humid regions. Adaptation strategies must therefore account for the

41   hydraulic memory of groundwater systems which can buffer climate change impacts on water

42   resources in many regions, but may also lead to a long, but initially hidden, legacy of

43   anthropogenic and climatic impacts on river flows and groundwater dependent ecosystems.

44

45

Text

47 Groundwater flow systems exist in dynamic balance with the climate, connecting interacting

48 zones of recharge (i.e. the replenishment of water in the subsurface) and discharge (the loss

49 of groundwater from the subsurface), with multiple feedbacks. As climate varies, changes in

50 the quantity and location of natural groundwater recharge lead to changes in groundwater

51 storage, water table elevations and groundwater discharge[1]. These changes in time and space

52 play a central role in controlling the exchange of moisture and energy across the Earth's land

53 surface[5,6] and connect processes critical to, for example, hydro-ecology, as well as carbon and

54 nutrient cycling[7]. Climate-groundwater interactions may also have played a key role in the

55 evolution of our own and other species[8] and continue to be critical in setting the availability

56 of water for abstraction by humans in coupled food-water-energy systems[1]. Recent global

57 mapping of water table depths[9] and the critical zone[10] suggest where interactions of climate

58 and groundwater may be most tightly coupled. However, they do not resolve where

59 groundwater systems are most sensitive to changes in climate and vice versa, or the

60 timescales over which such changes may occur.

61 Here, we derive and combine global scale analytical groundwater model results and other

62 hydrologic data sets to provide the first global assessment of the sensitivity of groundwater

63 systems to changes in recharge in both space and time (Figure 1), and discuss their utility as

64 an emergent constraint in understanding and modelling groundwater interactions with climate

65 and other Earth systems at the global scale.

66 We have characterized the mode of groundwater-climate interactions as being either

67 principally bi-directional or uni-directional using an improved formulation of the water table

68 ratio (*WTR*)[11,12] mapped globally at high resolution (Figure1a, Figure S1-2). The *WTR* is a

69 measure of the relative fullness of the subsurface and thus the extent of the water table's

70 interactions with topography. Values of *WTR*>1 indicate a topographic control on water table

71   conditions broadly correlating to shallow (<10 metres below ground level, m bgl) water table

72   depths (*WTD*s) globally (see Methods and Figure S3). This is indicative of a prevalently bi-

73   directional mode of groundwater-climate interaction (Figure 1c) where the climate system

74   can both give to the groundwater system in the form of recharge, and receive moisture back

75   via evapotranspiration if *WTD*s are shallow enough.

76   The land surface in such regions rejects a proportion of the potential recharge, and

77   groundwater can have a limiting control on land-atmosphere energy exchanges[5]; a tight two-

78   way coupling between groundwater and surface water is also common. In contrast, in

79   'recharge controlled' areas where *WTR*<1, water tables are more disconnected from the

80   topography and, while groundwater may still receive recharge from the land-surface, the

81   extent of two-way interaction between climate and groundwater is limited and the mode of

82   interaction is predominantly uni-directional (Fig. 1c).

83   We find that regions where *WTR*>1 cover around 46% of the Earth's land area (see Methods,

84   Figure 1a,b) and contribute to the large, but until recently underestimated, extent of

85   groundwater-vegetation interactions globally[10,13,14]. Consistent with previous regional

86   analyses and the form of the governing equation (see Methods), our results indicate that bi-

87   directional interactions are more likely to occur in areas with high humidity, subdued

88   topography and/or low permeability. In contrast, regions with *WTR*<1 are more common in

89   drier climates or more mountainous topography[11].

90   In order to assess the large scale temporal sensitivity of climate-groundwater interactions we

91   have used an analytical groundwater solution to quantify groundwater response times (*GRT*s)

92   globally and at high resolution. *GRT* is a measure of the time it takes a groundwater system to

93   re-equilibrate to a change in hydraulic boundary conditions[15]. For example, the *GRT*

94   estimates the time to reach an equilibrium in baseflow to streams (or other boundaries) after a

95   change in recharge rate, potentially from climate or land use change. Our results indicate that

96   groundwater often has a very long hydraulic memory with a global median *GRT* of nearly

97   6000 yrs, or approximately 1200 yrs when hyper-arid regions, where recharge is <5 mm/y,

98   are excluded (Figure 1d,e). Only 25% of Earth's land surface area has response times of less

99   than 100 yrs (herein called 'human timescale'). However, this is equivalent to nearly 44% of

100 global groundwater recharge flux, calculated by aggregating contemporary recharge over the

101 land area where *GRT*<100 y, expressed as a proportion of the total global recharge. Around

102 21% by area have uni-directional climate-groundwater interactions and response times on

103 human timescales, mostly associated with high permeability geology suggesting a strong

104 lithological control (Figure 2a).

105 The remainder (4%) in areas with bi-directional climate-groundwater interactions are mostly

106 located in the humid, lowland, tropical regions with unconsolidated sediments (e.g. Amazon

107 and Congo Basins, Indonesia), low-lying coastal areas (e.g. Florida Everglades, Asian mega-

108 deltas) or in high latitude, low topography humid settings (e.g. northeastern Canada, parts of

109 northern Europe).

110 A powerful advantage of using analytical groundwater equations such as the *WTR* is that they

111 allow us to directly assess the spatial sensitivity of the mode of climate-groundwater

112 interactions. By taking the derivative of *WTR* with respect to recharge (Figure S4) we have a

113 measure of the sensitivity of the relative fullness of the subsurface to changes in recharge (see

114 Methods). Our results indicate that the mode of climate-groundwater interaction is very

115 insensitive to relative changes in recharge (Figure 2b, Figure S5), with only 5% of the Earth's

116 land surface switching mode for a 50% relative change in recharge rate. This represents a

117 large change in natural groundwater recharge in the context of projections for the coming

118 century[16]. However, when absolute recharge rate changes are considered, more sensitivity is

119 apparent and a pattern emerges (Figure S6-7) that indicates the strong inverse relationship

120 between the spatial and temporal sensitivity of groundwater systems to changes in recharge

121 that we observe (Figure 3b). At small, local scales our calculations may have relatively large

122 uncertainties, stemming from the uncertainties in global data sets used for the analysis

123 particularly for hydraulic conductivity (see Methods). However, at the larger scales

124 considered here, Monte Carlo Experiments (MCE) indicate that, once the variance in each

125 parameter is combined, the global estimates have relatively small standard deviations

126 (Figures 1-2, S2).

127 The global pattern of *GRT* (Figure 1d) indicates a propensity for longer hydraulic memory in

128 more arid areas. Despite the expected scatter due to geomorphological and lithological

129 heterogeneity, there is a power law relationship between median *GRT* and groundwater

130 recharge (*R*) such that $GRT \propto 1/R^y$ with y ~ 2 (Figure 3a). This discovery is not directly

131 expected from the form of the governing equations but is rather an emergent property of

132 groundwater system interactions with the Earth's land surface and climate system. The

133 principal control on the observed power law is the distribution of perennial streams

134 (Figure S8) to which the *GRT* is most sensitive, and which itself is strongly controlled by

135 climate (Figure S9-11). How to characterize, quantitatively, this climatic control on the

136 perennial stream distributions is a pertinent question for further hydro-geomorphological

137 research.

138 We should not therefore expect *GRT*s to be static nor consider them as 'time constants'

139 despite being mathematically equivalent to other diffusion processes. Rather, *GRT*s will

140 evolve in time as both climate and geology vary the geometry and hydraulic properties of

141 groundwater flow systems. This will occur over long but diverse timescales associated with

142 changing river geometries.

143 Despite its importance, most global climate, Earth system, land surface and global hydrology

144 models exclude groundwater or do not allow groundwater to flow between model grid cells[18-

145 20]. While our results suggest that the spatial distribution of the mode of climate-groundwater

146   interactions may be rather static over century long timescales, we have shown that nearly a

147   half of the world's groundwater flux is responsive on 100 y timescales. Hence in order to

148   capture the important mass and energy transfers correctly, which may affect regional

149   precipitation and temperature dynamics[5,6], lateral flow circulation of groundwater must be

150   incorporated into the next generation of global models rather than assuming within-grid-cell

151   hydrological closure of the water budget as is currently often assumed[21-23]. Our *GRT*

152   calculations provide direct estimates of spin-up times to improve groundwater-enabled global

153   models, without having to use the currently employed methods of extrapolation[22]. Given the

154   long *GRT*s present over much of the Earth's land-surface, defining initial conditions with an

155   equilibrium water table calculated for present-day climate conveniently, but wrongly,

156   assumes stationarity in groundwater levels and fluxes. Since groundwater is known to be the

157   part of the hydrological system that takes longest to achieve equilibrium[24], new approaches

158   that incorporate the existence of long term transience should continue to be developed[25].

159   The global distribution of *GRT*s suggests that widespread, long-term transience in

160   groundwater systems persists in the present day due to climate variability since at least the

161   late Pleistocene in many semi-arid to arid regions (Figure 3a). This is consistent with

162   observations of larger than expected groundwater gradients, given the current low recharge,

163   that have been observed in present day arid zones[25]. While groundwater residence time and

164   groundwater response time are fundamentally different concepts, we also note the

165   correspondence between high *GRT* and significant volumes of fossil-aged groundwater

166   storage in arid regions[2,26]. The outcome of this result is that groundwater discharge to oases,

167   rivers or wetlands in otherwise dry landscapes will be particularly intransient in comparison

168   to climate change, in as much as climate controls the variations in groundwater recharge.

169   However, our results also indicate that groundwater response times tend to be greater in

170   regions where water tables are most sensitive to changes in recharge (Figure 3b). This

171 follows from the fact that both the groundwater response time and the derivative of the water

172 table ratio share a strong dependence on the square of the distance between perennial streams

173 (L, compare Equations 10 and 14).

174 Away from these more arid contexts, the responsiveness of groundwater systems has recently

175 been demonstrated to be as important as climate controls for the development of hydrological

176 drought[27]. For example, low GRT systems tend to enhance the speed of propagation of

177 meteorological drought through to hydrological drought whereas higher GRT systems

178 attenuate climate signals to a greater extent but also show greater lags in recovery from

179 drought. Thus, even within relatively small geographic areas, geological variations can lead

180 to very different drought responses even under similar climate variability. By way of a

181 specific example, increasing lags between meteorological and hydrological drought indicators

182 have been observed between the two most significant aquifers in the UK[28] in a manner

183 consistent with what would be expected from our estimates of GRT (i.e. Cretaceous Chalk

184 limestone - GRTs of months to years, Permo-Triassic sandstone – GRTs of years to 100s

185 years, Figure 1d).

186 Our analysis therefore provides a new framework for understanding global water availability

187 changes under climate change. First, the discovery of a power law relating groundwater

188 recharge and GRT suggests that important areas of groundwater discharge in naturally water

189 scarce parts of the world are likely to be more resilient to climate fluctuations than humid

190 areas. However, where groundwater response times are higher, water tables also tend to be

191 most sensitive to changes in recharge in the long term. Hence, accounting appropriately for

192 groundwater-climate interactions within analyses of global water scarcity in the context of

193 climate change is thus of great importance when explicitly considering the contribution of

194 groundwater storage changes[29]. Second, the long memory of groundwater systems in

195 drylands also means that abrupt (in geological terms) changes in recharge or widely

196 distributed groundwater abstraction will leave longer legacies. There may also be initially

197 'hidden' impacts on the future of environmental flows required to sustain streams and

198 wetlands in these regions. It is critical therefore that climate change adaptation strategies

199 which shift reliance to groundwater[1] in preference to surface water should also take account

200 of lags in groundwater hydrology[30] and include appropriately long timescale planning

201 horizons for water resource decision making. Third, robust assessments of the impact of

202 climate change on hydrological drought require estimates of 'groundwater responsiveness' [27].

203 The timescale of such responses can be directly informed by our results and improve the

204 decision making process with regard to adaptation strategies to changing drought frequencies

205 under climate change.

206

207 **Figure Captions**

208 **Figure 1**. **Global distributions of water table ratios (*WTR*) and groundwater response times (*GRT*) with**

209 **their conceptual interpretation as metrics of climate-groundwater interactions.** (**a**) Global map of

210 log(*WTR*) with hyper-arid regions of recharge (*R*) < 5 mm/y shaded grey[17]. (**b**) Frequency distribution of global

211 values of log(*WTR*). (**c**) Conceptual model for *WTR* as a metric for either bi-directional or uni-directional

212 groundwater-climate interactions - *WTR* is dependent on *R*, terrain rise (*d*), distance between perennial streams

213 (*L*) and the saturated thickness of the aquifer (*b*). (**d**) Global map of log(*GRT*). (**e**) Frequency distribution of

214 global values of *GRT* - median 5727 yrs (standard deviation, σ = 376 yrs), or 1238 yrs (σ = 92 yrs) when hyper-

215 arid regions are excluded. (**f**) Conceptual model of *GRT* as a metric of the temporal sensitivity of groundwater-

216 climate interactions.

217
218 **Figure 2. Global distributions of the temporal and spatial sensitivity of the mode of climate-groundwater**

219 **interactions.** (**a**) Temporal sensitivity: percentage of uni-directional and bi-directional groundwater systems, by

220 area globally, that will re-equilibrate significantly to changes in recharge on the timescale of <100 y or >100 y.

221 (**b**) Spatial sensitivity: percentage of the global area that would change mode from bi-directional to uni-

222 directional climate-groundwater interactions, or vice versa, for a relative change of 50% in recharge, given an

223 unlimited amount of time. Mapped values use the baseline parameter set (see Methods). The median percentage

224   coverage of Earth's landmass for each category from the Monte Carlo Experiments is labelled in the key with

225   standard deviations in percentage coverage shown in brackets. Grey areas represent contemporary recharge

226   <5 mm/y (ref[17]).

227

228   **Figure 3. Global quantitative inter-relationships between climate and the temporal (*GRT*) and spatial**

229   **(*WTR*) sensitivity of groundwater-climate interactions. (a)** Globally, median *GRT* values scale approximately

230   with the inverse of recharge (*R*) squared. Relationships between recharge and aridity index categories are shown

231   on the top axes as derived in Figure S12. Box extents are at 25-75% percentiles, with Tukey whiskers and

232   outliers. Histograms within each box represent median *GRT* values from each MCE realisation. **(b)** The

233   sensitivity of climate-groundwater interactions in time (*GRT*) and space (*dWTR*/*dR*) are log-correlated. Each

234   point uses median values for a geographic location from the MCE realisations. Inset plots are frequency

235   distributions of the slope and r^2 derived from linear regressions carried out for each realisation indicating

236   consistency in the relationship across the uncertainty range.

237

238   **References**

239   1   Taylor, R. G. *et al.* Ground water and climate change. *Nature Climate Change* **3**, 322-

240   329 (2013).

241   2   Jasechko, S. *et al.* Global aquifers dominated by fossil groundwaters but wells

242   vulnerable to modern contamination. *Nature Geoscience* **10**, 425-429 (2017).

243   3   Döll, P. Vulnerability to the impact of climate change on renewable groundwater

244   resources: a global-scale assessment. *Environmental Research Letters* **4**, 035006

245   (2009).

246   4   Green, T. R. *et al.* Beneath the surface of global change: Impacts of climate change on

247   groundwater. *Journal of Hydrology* **405**, 532-560 (2011).

248   5   Maxwell, R. M. & Kollet, S. J. Interdependence of groundwater dynamics and land-

249   energy feedbacks under climate change. *Nature Geoscience* **1**, 665-669 (2008).

250   6   Maxwell, R. M. & Condon, L. E. Connections between groundwater flow and

251   transpiration partitioning. *Science* **353**, 377-380 (2016).

252   7   Cole, J. J. *et al.* Plumbing the global carbon cycle: integrating inland waters into the

253   terrestrial carbon budget. *Ecosystems* **10**, 172-185 (2007).

254   8   Cuthbert, M. *et al.* Modelling the role of groundwater hydro-refugia in East African

255   hominin evolution and dispersal. *Nature Communications* **8** (2017).

256   9   Fan, Y., Li, H. & Miguez-Macho, G. Global patterns of groundwater table depth.

257   *Science* **339**, 940-943 (2013).

258   10   Xu, X. & Liu, W. The global distribution of Earth's critical zone and its controlling

259   factors. *Geophysical Research Letters* **44**, 3201-3208 (2017).

260   11   Gleeson, T., Marklund, L., Smith, L. & Manning, A. H. Classifying the water table at

261   regional to continental scales. *Geophysical Research Letters* **38** (2011).

262   12   Haitjema, H. M. & Mitchell   Bruker, S. Are water tables a subdued replica of the

263   topography? *Groundwater* **43**, 781-786 (2005).

264   13   Koirala, S. *et al.* Global distribution of groundwater   vegetation spatial covariation.

265   *Geophysical Research Letters* **44**, 4134-4142 (2017).

266   14   Schenk, H. J. & Jackson, R. B. Mapping the global distribution of deep roots in

267   relation to climate and soil characteristics. *Geoderma* **126**, 129-140 (2005).

268   15   Carr, E. & Simpson, M. Accurate and efficient calculation of response times for

269   groundwater flow. *Journal of Hydrology* **558**, 470-481 (2017).

270   16   Döll, P., Kaspar, F. & Lehner, B. A global hydrological model for deriving water

271   availability indicators: model tuning and validation. *Journal of Hydrology* **270**, 105-

272   134 (2003).

273   17   Döll, P. & Fiedler, K. Global-scale modeling of groundwater recharge. *Hydrology and*

274   *Earth System Sciences* **12**, 863-885 (2008).

275   18   Döll, P., Douville, H., Güntner, A., Schmied, H. M. & Wada, Y. Modelling

276   freshwater resources at the global scale: Challenges and prospects. *Surveys in*

277   *Geophysics* **37**, 195-221 (2016).

278   19   Sood, A. & Smakhtin, V. Global hydrological models: a review. *Hydrological*

279   *Sciences Journal* **60**, 549-565 (2015).

280   20   Wood, E. F. *et al.* Hyperresolution global land surface modeling: Meeting a grand

281   challenge for monitoring Earth's terrestrial water. *Water Resources Research* **47**

282   (2011).

283   21   Koirala, S., Yeh, P. J. F., Hirabayashi, Y., Kanae, S. & Oki, T. Global　scale land

284   surface hydrologic modeling with the representation of water table dynamics. *Journal*

285   *of Geophysical Research: Atmospheres* **119**, 75-89 (2014).

286   22   Milly, P. C. *et al.* An enhanced model of land water and energy for global hydrologic

287   and earth-system studies. *Journal of Hydrometeorology* **15**, 1739-1761 (2014).

288   23   Schaller, M. F. & Fan, Y. River basins as groundwater exporters and importers:

289   Implications for water cycle and climate modeling. *Journal of Geophysical Research:*

290   *Atmospheres* **114** (2009).

291   24   Ajami, H., McCabe, M. F., Evans, J. P. & Stisen, S. Assessing the impact of model

292   spin　up on surface water　groundwater interactions using an integrated hydrologic

293   model. *Water Resources Research* **50**, 2636-2656 (2014).

294   25   Schulz, S. *et al.* Improving large-scale groundwater models by considering fossil

295   gradients. *Advances in Water Resources* **103**, 32-43 (2017).

296   26   Befus, K. M., Jasechko, S., Luijendijk, E., Gleeson, T. & Cardenas, M. B. The rapid

297   yet uneven turnover of Earth's groundwater. *Geophysical Research Letters* **44**, 5511–

298   5520 (2017).

299 27   Van Lanen, H. A. J., *et al*. Hydrological drought across the world: impact of climate

300   and physical catchment structure. *Hydrology and Earth System Sciences* **17**, 1715-

301   1732 (2013).

302 28   Bloomfield, J. P., & Marchant, B. P. Analysis of groundwater drought building on the

303   standardised precipitation index approach. *Hydrology and Earth System Sciences* **17**,

304   4769-4787 (2013).

305 29   Damkjaer, S. & Taylor, R. The measurement of water scarcity: Defining a meaningful

306   indicator. *Ambio* **46**, 513-531 (2017).

307 30   Alley, W. M., *et al*. Flow and storage in groundwater systems. *Science* **296**, 1985-

308   1990 (2002).

309

320

321 **Author Contributions**

322 The idea for the paper was conceived by MOC and TG. Analyses were by all authors. The

323 manuscript was written by MOC with input from all authors.

324

Data Availability statement

Once the paper is accepted the main data outputs (i.e. *WTR* and *GRT* digital maps) will be made freely available for download via an online data repository and a link included in the final published version of the paper.

331 **METHODS**

332 **Derivation of Equations**

333 *Governing groundwater flow equations*

334 The governing equations were formulated by considering an ideal homogeneous, horizontal

335 unconfined aquifer bounded at one end ($x = L/2$) by a stream assumed to be a constant head

336 boundary and at the other ($x = 0$) by a no-flow boundary representing a flow divide

337 (Figure S13). The one-dimensional (Boussinesq) equation of groundwater flow for such an

338 aquifer receiving homogeneous recharge can be given as follows:

339
$$\frac{\partial}{\partial x}\left(Kh\frac{\partial h}{\partial x}\right) = S\frac{\partial h}{\partial t} - R(t) \tag{1}$$

340 where K is hydraulic conductivity [LT^{-1}], S is storativity [-], $h(x,t)$ is hydraulic head [L], t is

341 time [T], x is distance [L] and $R(t)$ is groundwater recharge [LT^{-1}].

342 If changes in transmissivity due to fluctuations in groundwater heads are assumed to be

343 negligible, Equation (1) may be linearised as follows:

344
$$T\frac{\partial^2 h}{\partial x^2} = S\frac{\partial h}{\partial t} - R(t) \tag{2}$$

345 where T is transmissivity [L^2T^{-1}], and $T = KH$, with H the average saturated thickness [L].

346 The lateral boundary conditions are as follows:

347
$$\frac{\partial h(0,t)}{\partial x} = 0 \, , \, h\left(\frac{L}{2}, t\right) = b \tag{3}$$

348 The parameter L is thus a characteristic length equivalent to the distance between perennial

349 streams which act as fixed head groundwater discharge boundaries.

350 *Water table ratio (WTR) derivations*

351   For steady state flow, where $h(x,t)$ becomes $h(x)$, the solution to Equation 1 for the stated

352   boundary conditions is:

353    $$h(x) = \left(b^2 + \frac{R}{K}\left(\frac{L^2}{4} - x^2\right)\right)^{0.5} \qquad (4)$$

354   At the flow divide, $x = 0$, therefore:

355    $$h(0) = \sqrt{b^2 + \frac{RL^2}{4K}} \qquad (5)$$

356   For steady state flow, the solution to the linearised form, Equation 2, for the stated boundary

357   conditions is:

358    $$h(x) = \frac{R}{2T}\left(\frac{L^2}{4} - x^2\right) + b \qquad (6)$$

359   At the flow divide, $x = 0$, therefore:

360    $$h(0) = \frac{RL^2}{8T} + b \qquad (7)$$

361   The WTR is defined[12] as the ratio of the head at the flow divide above the fixed head

362   boundary (i.e. $h_0 - b$) to the maximum terrain rise above the fixed head boundary, d [L].

363   This yields a new, non-linearised, form of the WTR, from Equation 5 as follows:

364    $$WTR_{NL} = \frac{\sqrt{b^2 + \frac{RL^2}{4K}} - b}{d} \qquad (8)$$

365   For the linearised form, from Equation 7, and as originally given by ref [12], the WTR is:

366    $$WTR_L = \frac{RL^2}{8Td} = \frac{RL^2}{8KHd} \qquad (9)$$

367   Equations 8 and 9 become equivalent for combinations of small L or R, or large K.

368   All maps and analysis presented in this paper use the non-linear form of the WTR

369   (Equation 8) with the exception of Figure S1 where the two versions are compared, and

370   calculated using the *L* parameters derived using a minimum river discharge threshold of

371   0.1 m³/s. A comparison of global maps and frequency distributions for the linear and non-

372   linear forms are shown in Figure S1-2. The frequency distribution comparison (Figure S2)

373   shows that the new non-linear formulation has a narrower and more symmetric distribution

374   with a median closer to zero than the linearised form. This is indicative of its better physical

375   representation such that the extent of higher *WTR*s is limited by the feedback between higher

376   water table elevation and concomitant increases in transmissivity inherent in the non-linear

377   Boussinesq equation (Equation 1).

378   The *WTR* is a measure of the relative fullness of the subsurface and thus the extent of the

379   water table's interactions with topography. We have therefore used the *WTR* to characterize

380   the dominant mode of groundwater-climate interactions as being either principally bi-

381   directional or uni-directional based on whether they are 'topographically controlled'

382   (*WTR*>1) or 'recharge controlled' (*WTR*<1), respectively. This is a reasonable approximation

383   since a global comparison with water table depths (*WTDs*) (Figure S3) indicates that *WTR*>1

384   broadly correlates to shallow (<10 metres below ground level) water table conditions. This

385   condition is indicative of a prevalently bi-directional mode of groundwater-climate

386   interaction where the climate system can both give to the groundwater system in the form of

387   recharge, and receive moisture back where local variations in *WTD*s enable

388   evapotranspiration to occur from groundwater directly. In contrast, areas with *WTR*<1 show

389   increasingly large *WTD*s well beyond plant rooting depths leading to predominantly uni-

390   directional climate-groundwater interactions where the groundwater system receives recharge

391   from the climate system but there is more limited potential for feedback in the other direction.

392   The sensitivity of the *WTR* to changing recharge is given by differentiating Equation 8 with

393   respect to *R*:

394 $$\frac{dWTR_{NL}}{dR} = \frac{L^2}{8Kd} \left(b^2 + \frac{RL^2}{4K}\right)^{-0.5}$$ (10)

395 This equation represents the sensitivity of the maximum head to recharge relative to the

396 topography which can be understood as the sensitivity of the 'fullness' of the subsurface to

397 changes in recharge.

398 Following from Equations 8, we calculate the recharge required for the WTR to equal 1 for

399 every grid cell as:

400 $$R_{WTR=1} = \frac{4K}{L^2} (d^2 + 2db)$$ (11)

401 The difference between R and the values given in Equation 11 then gives an expression for

402 the change in recharge (ΔR) needed to effect a change in the WTR across the transition

403 between topography control (bi-directional climate-groundwater interactions) and recharge

404 control (unidirectional climate-groundwater interactions) modes. In absolute terms this is:

405 $$\Delta R_{abs} = R - R_{WTR=1}$$ (12)

406 and in relative terms it becomes:

407 $$\Delta R_{rel} = \frac{R - R_{WTR=1}}{R}$$ (13)

408 ***Groundwater response time (GRT) definition***

409 The groundwater response time is, in general terms, a measure of the time it takes a

410 groundwater system to respond significantly (as defined below) to a change in boundary

411 conditions[15,31-35] and is defined here as follows:

412 $$GRT = \frac{L^2 S}{\beta T}$$ (14)

413 where β is a dimensionless constant, T is transmissivity [L^2T^{-1}], S is storativity [-] and L is

414 the distance between perennial streams [L]. To illustrate why this equation defines a time of

18

415 response consider a groundwater mound such as that shown in Figure S13. Let the initial

416 shape of the mound (of maximum height A), due to some steady recharge, be given by:

417 $$h(x,0) = A.cos\left(\frac{\pi x}{L}\right) \tag{15}$$

418 If recharge suddenly ceases (i.e., a step change) then it can be shown, in the manner of ref[33],

419 that the solution to the linearised Equation 2 without recharge (i.e. $R(t)=0$) is:

420 $$h(x,t) = h(x,0).exp\left(-\frac{t}{GRT}\right) \tag{16}$$

421 for β is equal to π^2.

422 Hence, for this case, the GRT controls the timescale for the groundwater levels to decay

423 exponentially to reach 63% re-equilibrium after a change in boundary (recharge) conditions

424 (i.e., an "e-folding" timescale). This value for β was chosen in order to be consistent with

425 mathematically equivalent uses of 'time constants' (often denoted as τ), in other branches of

426 science.

427 As outlined by ref[34], comparing the timescale of a particular forcing to the GRT can be a

428 useful measure of the degree of transience a groundwater system will manifest in terms of

429 variations in lateral groundwater flow. However, there is an important difference to note in

430 the case of a step change in conditions, as used to define GRT in Equation 14, in comparison

431 with a periodic variation in the forcing recharge (of period P). For the step change case

432 outlined above, both heads and fluxes decay exponentially after the change in recharge.

433 However, in the periodic case, where $GRT \gg P$, variations in recharge lead to very stable

434 groundwater fluxes (including at the downstream lateral boundary) but large temporal

435 changes in groundwater head across much of the aquifer[35]. Thus, it is important to distinguish

436 between the control of GRT on the degree of transience in either heads or fluxes, depending

437 on the nature of the boundary conditions.

Spatial input data and manipulation

Global mapping of the distance between perennial streams (L)

440   The distance between perennial streams (*L*) was calculated using a globally consistent river

441   network provided by the HydroSHEDS database[36] which was derived from the 90 m digital

442   elevation model of the Shuttle Radar Topography Mission (SRTM). For this study, we

443   extracted the global river network from the HydroSHEDS drainage direction grid at 500 m

444   pixel resolution by defining streams as all pixels that exceed a long-term average natural

445   discharge threshold of 0.1 cubic meters per second, resulting in a total global river length of

446   29.4 million kilometers. Smaller rivers with flows below this threshold were excluded as they

447   are impaired by increasing uncertainties in the underpinning data. However, the sensitivities

448   of the most important results of this paper to the chosen threshold are considered in our

449   uncertainty analysis below. Estimates of long-term (1971-2000) discharge averages have

450   been derived through a geospatial downscaling procedure[37] from the 0.5° resolution runoff

451   and discharge layers of the global WaterGAP model (version 2.2, 2014) a well-documented

452   and validated integrated water balance model[16,38]. Only perennial rivers were included in the

453   assessment; intermittent and ephemeral rivers were identified through statistical discharge

454   analysis (lowest month of long-term climatology is 0) and extensive manual corrections

455   against paper maps, atlases and auxiliary data, including the digital map repository of

456   National Geographic[39]. *L* was calculated for every pixel of the landscape (Figure S8) by

457   identifying the shortest combined Euclidean (straight-line) distance between two river

458   locations at opposing sides of the pixel. Neighbourhood low pass filters (5x5 kernel size)

459   were applied to remove outlier pixels and speckling. All calculations were performed in

460   ESRI© ArcGIS environment using custom-made scripts.

461   *Global mapping of the water table ratio (WTR), groundwater response times (GRT) and*

462   *other expressions*

463 Global *WTR* maps were created from the above equations using: the recharge rate (R in m/y),

464 based on ref[17], a minimum saturated thickness of the aquifer (b) set to 100 m (refs[40,41]), the

465 distance between two perennial streams (L, in m, as described above), intrinsic permeability

466 values (m^2) reported in ref[40] were converted to hydraulic conductivity (m/s) by assuming

467 standard temperature and pressure (1 x 10^7 multiplication factor) and then converted to units

468 of m/y. The maximum terrain rise between rivers (d, in m) was based on the range of

469 elevations in the 250m GMTED2010 data set[42].

470 The *GRT* was mapped using the same L data and hydraulic conductivity values as for the

471 *WTR* calculations. Transmissivity (T, m^2/y) was calculated by multiplying the hydraulic

472 conductivity with a fixed saturated thickness of 100 m (refs[40,41]). It was assumed that

473 storativity (S) for unconfined aquifers is dominated by the specific yield and that this can be

474 approximated by mapped porosity values[45]. Owing to the significant uncertainties in these

475 assumptions for calculating T and S values the parameters were subjected to a Monte Carlo

476 analysis as described below.

477 Each of the data sets was prepared to match a global equal-area projection with a grid size of

478 1 km x 1 km, and the calculations of the data sets were performed in ArcGIS. To avoid

479 mathematical problems, for zero values of d and R, 1 and 0.00001 were added, respectively.

480 For *WTR* estimates, regions where contemporary groundwater recharge was estimated as < 5

481 mm/y (ref[17]) were excluded from the analysis due to the increasingly large relative

482 uncertainties in recharge below this range, and the resulting unrealistic sensitivity of the

483 resulting *WTR* estimates. For deriving the frequency distributions and comparisons of

484 parameters from the range of derived geo-spatial data sets, point values were taken from each

485 raster of interest for 10,000 randomly distributed locations across the Earth's land-surface.

486 Global distributions of the parameters d, K and S are given in Figure S10 and relationships

487 between *R* and *L*; *d* and *WTR*; and *R* and *WTR* are explored in Figure S9, and Figures S11,

488 respectively. All areal calculations ignore the Antarctic landmass.

489 Although we have made best use of coherent available global datasets at high (1 km)

490 resolution for the calculations, our results are intended for appropriate large scale

491 interpretation, not detailed local analysis.

492 **Justification of the model assumptions**

493 Our calculations are based on mapped surface lithology only and, as such, they represent a

494 first estimate of the response of unconfined groundwater across the global land surface. The

495 more complex responses of regional or local confined aquifers, which may be locally

496 important to discerning groundwater-climate interactions, are not considered. However, such

497 confined aquifers only cover around 6-20% of the Earth's surface[43], are often located in more

498 arid parts of the world and are, by definition, inherently less connected to the land surface and

499 climate-related processes.

500 Using 1-D analytical solutions to the groundwater flow equations gives a powerful advantage

501 over the use of more complex models in enabling the sensitivity of the key parameters

502 controlling patterns and timescales of climate-groundwater interactions to be analysed

503 analytically. This, for example, allows us to sample the entire parameter space directly rather

504 than a restricted subset via a limited ensemble of more computationally expensive numerical

505 model runs. Equation 1 assumes the validity of the Dupuit-Forchheimer approximation

506 whereby the water table is assumed to be a true free surface governed by effective hydraulic

507 parameters and that water pressure in the direction normal to the flow is approximately

508 hydrostatic. This is a good approximation when the ratio of the lateral extent of the average

509 saturated depth is more than approximately 5 times its depth[12], i.e. $H/(L/2) < 0.2$ (see

510 Figure S13). Calculating the maximum saturated depth h_{max} as the smaller of $d+b$ or h_0, and

approximating the average saturated depth as $(h_{max} + b)/2$, we find that the criterion

$H/(L/2) < 0.2$ is met in 96% of our global grid calculations. Locations which fail this test are

all in mountainous regions where Equation 1 cannot account accurately for steep hillslope

groundwater hydraulics and hence our results may be less reliable in such areas.

The *GRT* is a parameter which consistently appears in solutions to the groundwater flow

equations and has been used for decades[32] as a robust estimate for the timescale of re-

equilibration of a groundwater system following a change in boundary conditions[8,15,30-35,44-48].

Thus it is an appropriate metric for long term transience which is currently impossible to

model in state of the art coupled groundwater-surface water models, which are limited to

short run times even for regional scale analyses due to their massive computational demands.

More realistic aquifer geometries and initial water table configurations lead to behaviours

which are more complex than the case of a simple exponential decay[46], and non-uniform flow

fields (strong convergence or divergence) can also lead to variations in *GRT* (refs[44,47,48]). We

have therefore included these factors in an uncertainty analysis as outlined below.

While the models used here cannot represent the detailed process interactions in the way that

a distributed fully coupled 3-D model would, they have a strong theoretical basis and show

consistency with other large scale studies based on very different model assumptions and data

sets. Justification for the approach of using *WTR* as a proxy for the mode of climate-

groundwater interaction is given in at least four ways. First, at global scale, similarities of

WTR with shallow *WTD* globally[9] are strong (Figure S3), given the very different model

assumptions and data sets employed in the two studies. Second, at a continental scale for the

contiguous US a recent study compared the results of a physically based, 3-D, fully coupled

surface water-groundwater model validated against water table depth data, against the *WTR*

metric[41]. The results show scatter as expected due to variations in the derivation of the

comparative characteristic length scales used in the comparison. However, general trends and

536 geographic patterns at a regional scale compare well between the WTD computed by the fully

537 coupled model and the calculated WTRs. Third, also at a continental scale for the contiguous

538 US, a systematic relationship has been shown between *WTR* and mean stream junction angles

539 which are indicative of a strong coupling between surface and subsurface[49]. Lastly,

540 comparisons of *WTR* calculations against a more complex 3-D regional groundwater flow

541 model, has indicated that the *WTR* is a robust indicator of groundwater's connection to the

542 land surface as it is a strong predictor of the propensity for local versus regional flow

543 conditions[50]. Our analyses thus allow us to make a robust first global scale estimate of the

544 sensitivity of climate-groundwater interactions, while enabling the range of uncertainty to be

545 fully and directly appreciated.

546 **Uncertainties and Monte Carlo experiments**

547 We ran 10,000 Monte Carlo experiments (MCE) at 10,000 randomly distributed locations

548 across the Earth's land-surface to investigate the range of uncertainty due to parameter

549 uncertainties as well as model structural simplifications.

550 Hydraulic conductivity (K) was allowed to vary log-normally within uncertainty ranges

551 defined in refs[40,50], this parameter having by far the highest uncertainty of any others used in

552 our calculations. Groundwater recharge (R) values were taken from ref[17] but allowed to vary

553 through a normal distribution with a standard deviation of 22% of this baseline, chosen

554 according to the difference with a contrasting global recharge distribution[52,53] commonly used

555 in other global hydrological calculations. Storativity (S) was sampled from a normal

556 distribution with standard deviations of 25% of the mapped value[53]. Although the absolute

557 error in the DEM used is only 1-2 m, we allowed the maximum terrain rise (d) to vary

558 normally with a standard deviation of 10% to allow for uncertainties due to gridding. The

559 minimum saturated thickness of the aquifer (b) was allowed to vary log-normally around

560 100 m with a standard deviation of 0.3 orders of magnitude. Sampled distributions were cut

561 off at zero to stop meaningless negatives being included in the calculations.

562 Parameter uncertainty in the distance between perennial streams (L), calculated from the

563 variation in L for an order of magnitude change in discharge threshold used to define the

564 stream network (from 0.1 to 1 m³/s), gives a median uncertainty of a factor of 1.9. However,

565 there is also additional uncertainty to L due to the choice of the one-dimensional groundwater

566 flow solutions applied, which ignore non-uniform (i.e. convergent or divergent) flow fields

567 which are common in real catchments. In order to account for the maximum likely range of

568 possible uncertainty, we have compared the 1-D analytical solutions used here to cases of

569 radial flow which represent an extreme 2-D non-uniform flow end-member for natural

570 groundwater flow systems. By equating the distance between perennial streams (L) to be

571 equal to the radius of the flow domain for the equivalent radial solutions, we can estimate the

572 impact of this choice on both *WTR* and *GRT*. For *WTR*, by replacing Equation 6 with Eq

573 30.11 from ref[54], the average error is approximately a factor of 2. For the *GRT*, comparison of

574 recession timescales for 1-D and radial flow cases (e.g. Appendix A of ref [46]) indicates a

575 similar level of uncertainty due to non-uniform flow as for the *WTR*. We therefore added a

576 log-normal variation in L with a standard deviation of 0.3 orders of magnitude to

577 accommodate the likely range of combined parameter and structural uncertainty.

578

579 **References (additional for Methods, numbering following on from main text references)**

580 31 Domenico, P. A. & Schwartz, F. W. *Physical and chemical hydrogeology*. Vol. 506

581   (Wiley New York, 1998).

582 32 Downing, R., Oakes, D., Wilkinson, W. & Wright, C. Regional development of

583   groundwater resources in combination with surface water. *Journal of Hydrology* **22**,

584   155-177 (1974).

585   33   Erskine, A. & Papaioannou, A. The use of aquifer response rate in the assessment of

586   groundwater resources. *Journal of Hydrology* **202**, 373-391 (1997).

587   34   Currell, M., Gleeson, T. & Dahlhaus, P. A new assessment framework for transience

588   in hydrogeological systems. *Groundwater* **54**, 4-14 (2014).

589   35   Townley, L. R. The response of aquifers to periodic forcing. *Advances in Water*

590   *Resources* **18**, 125-146 (1995).

591   36   Lehner, B., Verdin, K. & Jarvis, A. New global hydrography derived from spaceborne

592   elevation data. *Eos, Transactions American Geophysical Union* **89**, 93-94 (2008).

593   37   Lehner, B. & Grill, G. Global river hydrography and network routing: baseline data

594   and new approaches to study the world's large river systems. *Hydrological Processes*

595   **27**, 2171-2186 (2013).

596   38   Alcamo, J. *et al.* Development and testing of the WaterGAP 2 global model of water

597   use and availability. *Hydrological Sciences Journal* **48**, 317-337 (2003).

598   39   National Geographic, *Atlas of the World*. Ninth Edition edn, National Geographic

599   (2010).

600   40   Gleeson, T., Moosdorf, N., Hartmann, J. & Beek, L. A glimpse beneath earth's

601   surface: GLobal HYdrogeology MaPS (GLHYMPS) of permeability and porosity.

602   *Geophysical Research Letters* **41**, 3891-3898 (2014).

603   41   Condon, L. E. & Maxwell, R. M. Evaluating the relationship between topography and

604   groundwater using outputs from a continental-scale intergrated hydrology model.

605   *Water Resources Research* **51**, 6602-6621 (2015).

606   42   Danielson, J. J. & Gesch, D. B. Global multi-resolution terrain elevation data 2010

607   (GMTED2010). Report No. 2331-1258, (US Geological Survey, 2011).

608   43   de Graaf, Inge E.M., *et al.* A global-scale two-layer transient groundwater model:

609   Development and application to groundwater depletion. *Advances in water resources*

610   **102**, 53-67 (2017).

611   44   Rousseau Gueutin, P. *et al.* Time to reach near steady state in large aquifers. *Water*

612   *Resources Research* **49**, 6893-6908 (2013).

613   45   Rushton, K. R. & Redshaw, S. C. *Seepage and groundwater flow: Numerical analysis*

614   *by analog and digital methods*. (Chichester, 1979).

615   46   Cuthbert, M. Straight thinking about groundwater recession. *Water Resources*

616   *Research* **50**, 2407-2424 (2014).

617   47   Cuthbert, M. *et al.* Understanding and quantifying focused, indirect groundwater

618   recharge from ephemeral streams using water table fluctuations. *Water Resources*

619   *Research* **52**, 827-840 (2016).

620   48   Walker, G. R., Gilfedder, M., Dawes, W. R. & Rassam, D. W. Predicting Aquifer

621   Response Time for Application in Catchment Modeling. *Groundwater* **53**, 475-484
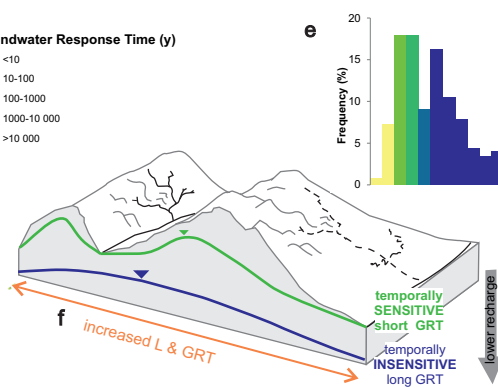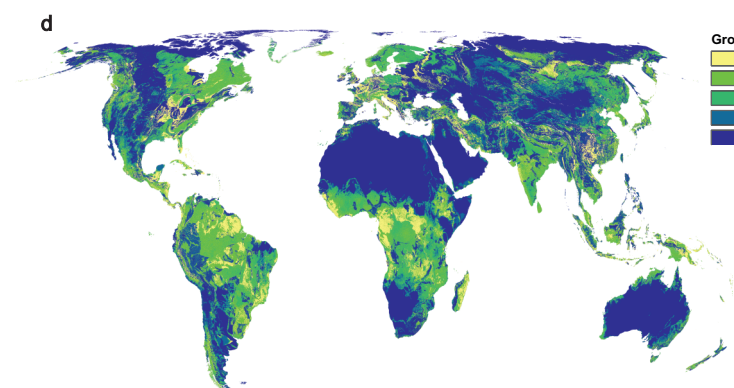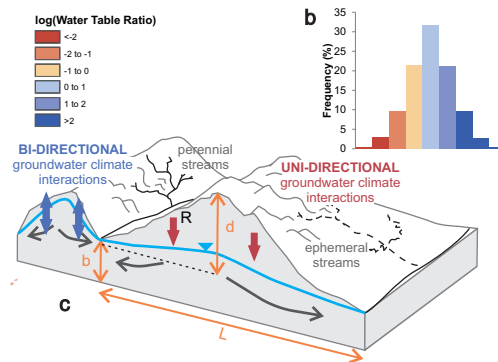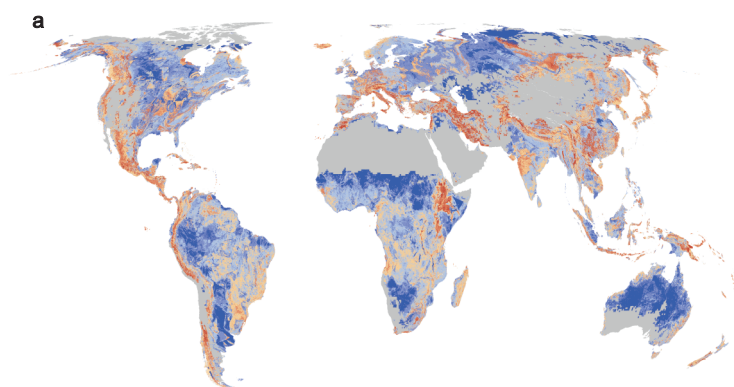
622   (2015).

623   49   Seybold, H., Rothman, D. H., & Kirchner, J. W. Climate's watermark in the geometry

624   of stream networks. *Geophysical Research Letters* **44**, 2272-2280 (2017).

625   50   Gleeson, T., & Manning, A. H. Regional groundwater flow in mountainous terrain:

626   Three dimensional simulations of topographic and hydrogeologic controls. Water

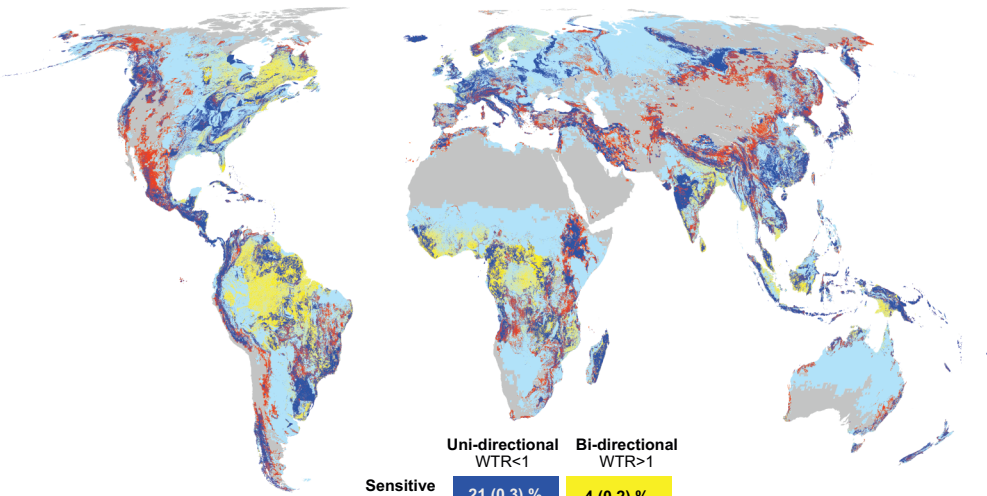627   Resources Research 44, W10403 (2008).

628   51   Gleeson, T., *et al*. Mapping permeability over the surface of the Earth. *Geophysical*

629   *Research Letters* **38**, L02401 (2011).

630   52   De Graaf, I. E. M., *et al*. A high-resolution global-scale groundwater model.

631   *Hydrology and Earth System Sciences* **19**. 823-837 (2015).

632   53   Wada, Y., *et al*. Global depletion of groundwater resources. *Geophysical Research*

633   *Letters* **37**, L20402 (2010).

634   54   Bruggeman, G.A., Analytical Solutions of Geohydrological Problems. *Developments*

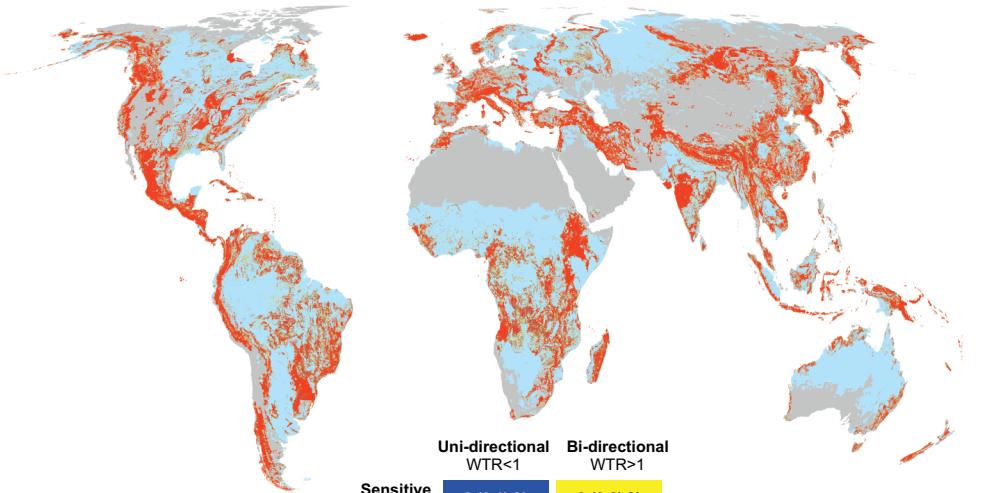635   *in Water Science* **46**, 3-959 (Elsevier, 1999)

a

log(Water Table Ratio)
- <-2
- -2 to -1
- -1 to 0
- 0 to 1
- 1 to 2
- >2

b

Frequency (%)

c

BI-DIRECTIONAL
groundwater climate
interactions

perennial
streams

UNI-DIRECTIONAL
groundwater climate
interactions

R

d

b

ephemeral
streams

L

d

Groundwater Response Time (y)
- <10
- 10-100
- 100-1000
- 1000-10 000
- >10 000

e

Frequency (%)

f

increased L & GRT

temporally
SENSITIVE
short GRT

temporally
INSENSITIVE
long GRT

lower recharge

a

	Uni-directional WTR<1	**Bi-directional** WTR>1	
Sensitive GRT<100 y	21 (0.3) %	4 (0.2) %	R<5 mm/y
Insensitive GRT>100 y	7 (0.2) %	42 (0.4) %	26 (0.1) %

b

	Uni-directional WTR<1	**Bi-directional** WTR>1	
Sensitive ΔR<50%	2 (0.1) %	3 (0.2) %	R<5 mm/y
Insensitive ΔR>50%	26 (0.3) %	42 (0.3) %	26 (0.1) %